Research Article Vol. 12, No. 7 / 1 Jul 2022 / Optical Materials Express 2508
Optical Materials EXPRESS

Advantages of YLF host over YAG in power scaling at cryogenic temperatures: direct comparison of Yb-doped systems

UMIT DEMIRBAS,[1,2,*] MARTIN KELLERT,[1] JELTO THESINGA,[1] SIMON REUTER,[1] FRANZ X. KÄRTNER,[1,3,4] AND MIKHAIL PERGAMENT[1]

[1]Center for Free-Electron Laser Science CFEL, Deutsches Elektronen-Synchrotron DESY, Notkestr. 85, 22607 Hamburg, Germany
[2]Laser Technology Laboratory, Department of Electrical and Electronics Engineering, Antalya Bilim University, 07190 Dosemealti, Antalya, Turkey
[3]Physics Department and The Hamburg Centre for Ultrafast Imaging, University of Hamburg, Luruper Chaussee 149, 22761 Hamburg, Germany
[4]The Hamburg Centre for Ultrafast Imaging, Luruper Chaussee 149, 22761 Hamburg, Germany
*uemit.demirbas@cfel.de

Abstract: We have investigated the cryogenic performance of Yb:YAG and Yb:YLF crystals in rod-geometry to understand the pros and cons of each material for the development of ultrafast lasers and amplifier systems. We have performed detailed spectroscopic (absorption, emission, lifetime), temperature, lasing, and thermal-lens measurements with Yb:YLF and Yb:YAG crystals under almost identical conditions. Our analysis has shown that despite the higher thermal conductivity of Yb:YAG, due to its smaller quantum defect, the peak/average temperatures reached under similar pumping conditions is lower in Yb:YLF crystals. Moreover, since the YLF host has a negative thermo-optic coefficient, that balances other positive contributions to thermal lensing, overall Yb:YLF rods possess a much weaker thermal lens than Yb:YAG under similar conditions. As a result of these benefits, we have shown that Yb:YLF rods perform better than Yb:YAG in cryogenic lasing experiments in terms of attainable power performance and laser output beam quality. In terms of gain per pass, the Yb:YAG medium is superior, however, the gain bandwidth is much broader in Yb:YLF systems that make it more suitable for ultrafast pulse laser/amplifier development. We have further shown that, the asymmetric thermal lens behavior of Yb:YLF favors laser operation in E//c axis over E//a axis. The comparison in this study has been performed in rod geometry and for Yb-doping, however, we believe that, to first order, the discussion could be extended to YAG/YLF laser systems doped with other ions (Pr, Nd, Er, Tm, Ho) and to other lasing geometries such as slab and thin-disk.

© 2022 Optica Publishing Group under the terms of the Optica Open Access Publishing Agreement

1. Introduction

Yb:YAG laser/amplifier systems are one of the main carrying pillars of high-power ultrafast technology [1,2], due to favorable spectroscopic characteristics of Yb-dopants and the thermo-mechanical strength of the YAG host [3–5]. Over the last decades, the progress in high-power laser diode technology has led to industrial-grade, cost-effective, multi-kW level diode systems for pumping. Moreover, thermal limitations observed in rod geometry have been overcome by employing several novel concepts, including usage of well-designed cooling jets [6], and employment of slab [7], crystal fiber [8], and thin-disk [9,10] geometries. As a result, state-of-the-art room-temperature Yb:YAG systems now produce sub-picosecond level pulses at kW average power levels [10–12].

#460445 https://doi.org/10.1364/OME.460445
Journal © 2022 Received 5 Apr 2022; revised 22 May 2022; accepted 30 May 2022; published 9 Jun 2022

Optical Materials EXPRESS

As an alternative/additional approach, Yb:YAG systems have also been operated at cryogenic temperatures [13–17]. Cooling the laser crystal not only improves the thermo-mechanical strength of the YAG host [18], but also improves the spectroscopic properties of the Yb-dopant [19], and hence providing significant advantages in terms of gain and power scaling. However, these benefits come at the expense of increased laser complexity (requirement to operate under vacuum at cryogenic temperatures etc. . .), and reduced gain bandwidth [14]. As a consequence of the reduced gain bandwidth, pulsewidths obtainable in cryogenic Yb:YAG amplifiers is limited to 4-5 ps level [20–23]. Hence, despite the advantages of cryogenic Yb:YAG systems in power/energy scaling, their intrinsic limitation in obtainable pulse width hinders performance in several ultrafast laser applications.

As an attractive alternative to Yb:YAG, Yb:YLF systems could offer broad gain bandwidths that ideally support generation/amplification of pulses down to sub-250-fs length even at cryogenic temperatures [24–31]. This broader emission comes at the expense of reduced emission cross section values; however, the longer upper state lifetime of Yb:YLF partially balances this drawback in terms of attainable gain. Additionally, the birefringent/biaxial nature of the YLF host minimizes depolarization loss and the different spectral and thermal properties in E//a and E//c axis enables the laser engineer to optimize the crystals used for the specific needs of the system, which is not possible in the case of the isotropic YAG host [4]. Furthermore, the YLF host possesses a weaker thermal lens (TL) due to its negative dn/dT coefficient [32–39], which enables implementation of higher average power systems with better beam quality, as it is already confirmed in earlier room-temperature studies with Nd:YLF [34, 36–45]. To our knowledge, literature lacks a comprehensive study comparing the pros and cons of YLF and YAG hosts at cryogenic temperatures. Especially, there is almost no comparative discussion of thermal lens behavior of Yb-doped YAG and YLF crystals, and current literature with comparative analysis primarily focuses on room-temperature Nd-based systems [32,33,46]. Without the presence of comparative data taken in almost identical systems, it is hard for researchers to look at independently performed studies and make design decisions.

Motivated by this need, we have performed detailed spectroscopic (absorption, emission, and lifetime), temperature, lasing, and thermal lens measurements with Yb:YAG and Yb:YLF rods at cryogenic temperatures under almost identical conditions. Our analysis has demonstrated that, despite the known advantages of the YAG host in terms of thermal conductivity, thermal expansion coefficient and fracture toughness, Yb:YLF systems provide better lasing performance compared to Yb:YAG in terms of power scalability and output beam quality. We have shown that this advantage is due to the lower quantum defect and weaker thermal lens observed in Yb:YLF, especially in its E//c axis.

The paper is organized as follows: In Section 2, we first describe the experimental methodology that is applied. Section 3 presents absorption, emission, fluorescence lifetime, crystal temperature, thermal lens and lasing data taken with cryogenic Yb:YLF and Yb:YAG systems under almost identical conditions. Finally, in Section 4, we finalize with a brief summary and provide an outlook for future cryogenic Yb:YLF systems.

2. Experimental approach

We used identical experimental conditions in our experimental campaign, as much as possible, to obtain a fair direct comparison between YAG and YLF hosts. Therefore, we employed Yb:YAG and Yb:YLF samples with almost identical specifications. All the samples used in this study have a Yb-doping of 1%: a concentration level that we found to be rather optimum in rod geometry. This doping is low enough to enable rather homogeneous distribution of heat load along a fairly long portion of the crystal, yet it is still high enough to enable sufficient absorption even at high pumping intensities [47,48]. One a-cut and one c-cut Yb:YLF crystals with 20 mm length and aperture sizes of 10×15 mm^2, and one Yb:YAG crystal with a length of 24 mm and an aperture

Optical Materials EXPRESS

size of 5×15 mm^2 are used in the experiments. These lengths (20-24 mm) still enable fairly good mode-matching between the laser and the low-brightness (large M^2) pump mode. The Yb:YLF crystals contain 3 mm long undoped endcaps diffusion-bonded on both ends, and hence the total crystal length is 26 mm. The Yb:YAG crystal has a 3 mm undoped cap on its front side only, and thus has a total length of 27 mm. The undoped endcaps enable minimization of surface bulging induced thermal lensing for both cases. All crystals are antireflection coated with a simple few-layer coating that is effective at the pump and laser wavelengths. The crystals are indium soldered from the top side to a multi-stage pyramidal cold head, which is cooled to cryogenic temperatures by boiling liquid nitrogen using a vacuum sealed dewar system. Hence, the cooling cross section surface is almost identical for Yb:YAG (27×15 mm^2) and Yb:YLF (26×15 mm^2). In the experiments the pump beam is located close to the top side of the crystals (Fig. 1), to minimize the thermal resistance of the system and to enable better cooling. Therefore, the different height of the Yb:YLF (10 mm) and Yb:YAG (5 mm) samples do not create much difference in cooling efficiency, as long as the distance between the pump light and cooling surface is kept equal.

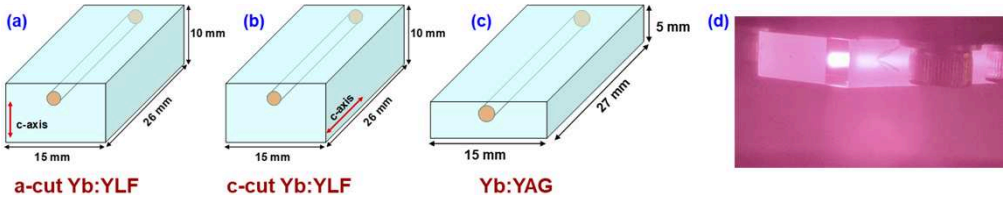

Fig. 1. Dimensions and orientations of the 1% Yb-doped (a) a-cut Yb:YLF, (b) c-cut Yb:YLF and (c) Yb:YAG crystals used in the experiments. The location of the pump mode within the crystals are also shown (shaded cylindrical area inside rectangular gain medium). The pump line upper edge was around 2 mm below the crystal upper surface in all cases. The crystals are indium soldered from their top side to a multi-stage pyramidal cold head that is cooled via direct contact with boiling liquid nitrogen. (d) Picture of the cryogenically cooled Yb:YAG crystal inside the dewar. The emission from the pump beam is also visible.

We have recently discussed the experimental methodology used in absorption, emission, and lifetime measurements of Yb:YLF and Yb:YAG crystals in detail in [49,50], and we will only provide a brief summary here. A home-built broadly-tunable (770-1110 nm) continuous-wave (CW) Cr:LiSAF laser [51] is used in the absorption and emission measurements. The Cr:LiSAF laser produced up to 100 mW of linearly polarized output with a spectral width below 0.1 nm at full-width at half-maximum (FWHM). For the absorption measurements, the Cr:LiSAF output beam (diameter: 1.3 mm) is sent through the sample's center. The incident and transmitted power levels are recorded carefully using a sensitive power meter (Thorlabs S121C). The absorption of the crystals at each wavelength is calculated after subtracting the background loss of the system. The temperature dependent emission spectra are measured at a 90° angle to the Cr:LiSAF beam propagation direction using a window at the side of the dewar. These measurements use a smaller excitation beam size of around 100 μm to minimize self-absorption effects (the crystals are also excited from their edge). In the case of Yb:YLF, a thin- film polarizer (Thorlabs LPNIRE100-B) is used for selecting the fluorescence emission in the relevant axis. A 3648 pixel CCD array (Toshiba TCD1304AP) based Ocean Optics spectrometer with a spectral resolution of 0.1 nm in the 900-1060 nm range is used for recording the fluorescence spectra. The emission cross section in absolute units is calculated using the modified Füchtbauer–Ladenburg formula. The temperature dependence of emission spectra is used to estimate the average crystal temperature and the procedure for this is outlined in detail in [52,53].

Optical Materials EXPRESS

We have used fiber-coupled, 960 nm and 940 nm laser diodes with peak powers of up to 3 kW as the excitation source in lifetime and lasing experiments of Yb:YLF and Yb:YAG, respectively. The pump modules employed 600 µm core diameter fibers with a numerical aperture (NA) of 0.22, and the pump output from the fiber tips are collimated with 72 mm focal length lenses (f1) and focused to a pump diameter of 2.08 mm using lenses with 250 mm focal length (f2). In typical emission lifetime measurements, crystals are excited with 200 µs long pump pulses with 2 kW of peak power at a repetition rate of 1 Hz (average incident power: 0.4 W). The fluorescence decay signal is measured at 90° to the direction of excitation beam, and a 1000 nm high-pass filter (Thorlabs, FELH1000) is implemented to cut out scattered pump light. A free-space 350 MHz Si detector (Thorlabs, DET10A) with a sub-20 µs response time is used to monitor the fluorescence decay signal. Pinholes with diameters between 10 µm and 2 mm are used to estimate of radiation-trapping free lifetimes.

In CW laser experiments, we have compared the performance of Yb:YAG and Yb:YLF crystals in two different cavities. In the initial experiments (Fig. 2 (a)), a very simple compact flat-flat cavity is implemented using a flat dichroic mirror (DM) and a flat output coupler. The total cavity length is around 30 cm, just long enough to contain the dewar system (named as a short cavity). The dichroic mirrors have a transmission > 95% for the pump wavelengths (940-960 nm) and have a reflectivity higher than 99.9% in the 990-1040 nm range. We have tested output couplers with transmissions of 10-80% for both materials and among these the optimum performance is obtained with around 25% coupling (obtainable slope efficiencies do not vary much for output coupling in the 20-60% range: details could be found in [47]). As in lifetime measurements, a pump spot diameter 2.08 mm is also employed in the lasing experiments (obtained via usage of f1-f2 telescope). In all the experiments, the Yb:YAG and Yb:YLF crystals absorbed more than 80% of the unpolarized pump light. Up to 1 kW of pump light was incident on the crystals (2.1 mm diameter spot), and despite the lower mechanical strength of YLF host, we have not observed any crystal fracture damage in our experiments, owing to the quality of thermal contact to the cold head.

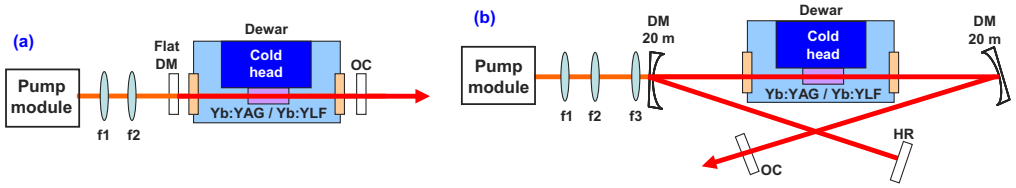

Fig. 2. Simplified schematic of the setups used in (a) short-cavity, and (b) long-cavity CW laser experiments with Yb:YAG and Yb:YLF. Short cavity: flat-flat configuration, long-cavity: x-shaped standing wave cavity with two curved dichroic mirrors. f1-f3: Lenses for pump coupling, DM: Dichroic mirror, HR: High reflectivity mirror, OC: Output coupler.

The CW laser performance of the Yb:YAG and Yb:YLF crystals are then compared in a long standing wave cavity, that is more sensitive to the pump induced thermal lensing in the gain element. This long cavity consisted of two 20 m radius of curvature curved dichroic mirrors, a flat high reflector and a flat output coupler (Fig. 2 (b)). For this cavity, the distance between the curved mirrors is around 70 cm, and due to the small working range of the f1-f2 telescope, another 150 mm focal length lens (f3) is necessary to re-image the pump beam inside the gain media (again to a spot diameter of 2.08 mm). Short and long arm lengths of 70 cm and 85 cm are employed, resulting in a cold cavity beam diameter of 2.1 mm at the center of the crystals and 2.02 mm at the output coupler. For this cavity, we have monitored the variation of the laser output beam profile with absorbed pump power level: (i) to probe the beam quality of the laser, and (ii) to estimate the induced thermal lens strength of the laser.

Optical Materials EXPRESS

Figure 3 shows a simplified schematic of the setup used to directly measure the thermal lens strength. We employed the same pump module system to obtain a 2.08 mm pump spot diameter at the center of the crystals. In order to explore the strength of the thermal lens, the system is probed with an Nd:YAG laser at 1064 nm. At this wavelength neither Yb:YLF nor Yb:YAG has gain at cryogenic temperatures. The probe beam profile is monitored using a high resolution (2048×2048 pixels) beam profiler camera (DAT-WinCamD-LCM). The collimated output of the probe beam has a size of around 3.7 mm diameter at the position of the beam profiler camera, which is positioned 1 m and 2 m after the crystal for the case of Yb:YAG and Yb:YLF crystals, respectively. We have first monitored the variation of the beam size with absorbed pump power level, and afterwards the strength of the thermal lens induced inside the laser crystal is estimated using simple ABCD matrix beam propagation formalism for Gaussian beams. Finally, the incident polarization of the probe beam is adjusted using a half-wave-plate in order to investigate the polarization dependence of the thermal lens strength.

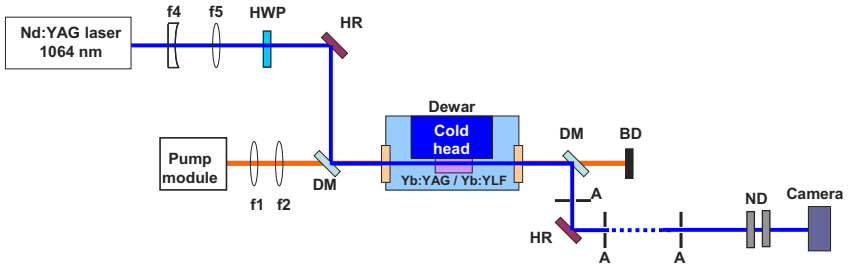

Fig. 3. Simplified schematic of the thermal lens measurement setup. The system measures the variation of the beam size of the collimated 1064 nm probe beam as a function of absorbed pump power. Usage of dichroic mirrors and several apertures along the path of the probe beam minimizes the presence of pump light near the beam profiler camera. HWP: Half-wave plate, DM: Dichroic mirror, A: Adjustable circular aperture, ND: Neutral-density filters, HR: High-reflector mirrors, BD: Beam dump.

3. Comparison of Yb:YAG and Yb:YLF

In this section, we will first present spectroscopic properties of Yb:YAG and Yb:YLF crystals at cryogenic temperatures and comparatively discuss their advantages and disadvantages for ultrafast laser/amplifier development. As the second step, based on this spectroscopic information, we will look at the variation of the quantum defect with temperature in these crystals, and directly estimate crystal temperatures under pumping conditions. Later, the cw laser performance of Yb:YAG and Yb:YLF will be compared in short and long cavity configurations. The section will be finalized by comparing thermal lenses of the different gain media.

3.1. Comparison of the absorption spectrum

Figure 4 shows measured absorption cross section spectra for the Yb:YAG and Yb:YLF crystals at temperatures of 78 K and 295 K. This data is taken with 1% Yb-doped samples and agrees reasonably well with previous reports in the literature [54–57]. From Fig. 4 (a), we see that, Yb:YAG has three strong absorption bands centered around 914 nm, 941 nm and 969 nm at room temperature. Among those bands, pumping at the zero-phonon line at 969 nm has advantages due to smaller quantum defect [58]. This line has a width of around 3 nm at room temperature, but it gets quite narrow at cryogenic temperatures: sub-0.1 nm at 78 K, and sub-0.5-nm at 150 K [59]. Current state-of-the-art high power (multi-kW) diodes have an emission bandwidth of around 2-3 nm (Fig. 2 in [60]), and hence the zero phonon line of Yb:YAG is not very suitable for pumping

Optical Materials EXPRESS

of cryogenic systems [61]. As a result, the 940 nm line, which is also rather broad at cryogenic temperatures (~3 nm at 78 K), is employed to pump cryogenic Yb:YAG systems [20–23].

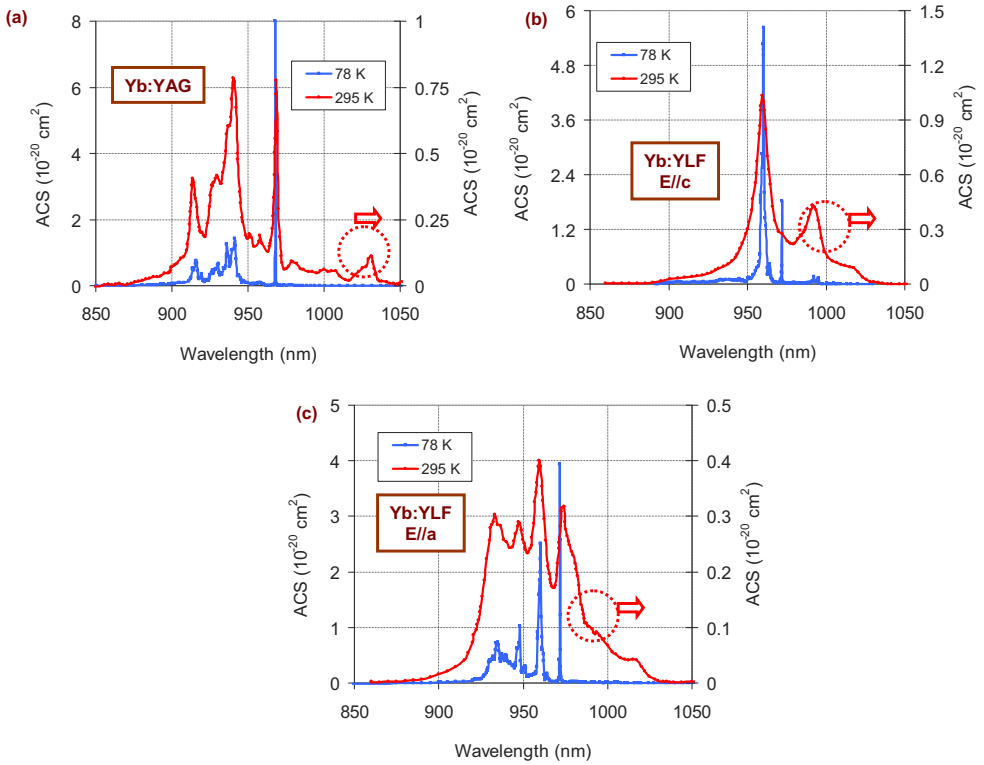

Fig. 4. Measured absorption cross section of (a) Yb:YAG, (b) Yb:YLF E//c axis and (c) Yb:YLF E//a axis at 78 K and 295 K.

In the case of room-temperature Yb:YLF, there are absorption peaks around 960 nm and 993 nm for E//c axis (Fig. 4 (b)), and around 933 nm, 948 nm, 960 nm and 974 nm in the case of E//a axis (Fig. 4 (c)). Note that, the E//a axis is broader, but it has lower peak cross section values. The zero-phonon line, which is located at around 971.5 nm in Yb:YLF is also rather narrow at cryogenic temperatures (sub-0.5 nm). As a result, the 960 nm line with a FWHM of around 1.5 nm is usually employed for efficient pumping of cryogenic Yb:YLF systems. Note that this transition is strong for both polarizations (5.6×10^{-20} cm^2 for E//c and 2.5×10^{-20} cm^2 for E//a at 78 K), which provides flexibility while pumping with unpolarized fiber-coupled laser diode systems. We refer the interested readers to [49] for further detailed data on temperature variation of absorption cross section in Yb:YLF, including the 960 nm transition.

From Fig. 4 (a), we see that the 940 nm line of Yb:YAG has a peak absorption coefficient of 1.4×10^{-20} cm^2 at 78 K, that is relatively low compared to the 960 nm line of Yb:YLF. We want to also mention that, due to its lower fluorescence lifetime, the absorption saturation intensity of Yb:YAG (15.1 kW/cm^2) is higher than for Yb:YLF (1.85 kW/cm^2 for E//c, 4.2 kW/cm^2 for E//a). Hence, it is harder to reach pump saturation in cryogenic Yb:YAG systems, which enables more efficient absorption at high pump intensities [62]. On the other hand, the pump saturation can be used to better distribute the thermal load in long laser crystals, which provides advantages to Yb:YLF in terms of thermal effects as we will see later. Lastly, under lasing/amplification conditions, the intracavity circulating laser beam will partially suppress the pump saturation effect via stimulated emission. Hence, the pump saturation effect is expected to create challenges only

Optical Materials EXPRESS

in some rare cases, where efficient extraction could not be achieved (e.g. in Yb:YLF amplifiers operating at low repetition rates).

3.2. Comparison of fluorescence lifetimes

The observed variation of effective fluorescence lifetime of Yb:YAG and Yb:YLF in the 78-300 K temperature range is shown in Fig. 5 (a). As we can see, the 1% Yb-doped YAG sample has a fluorescence lifetime of 1.02 ms at 78 K, which monotonically increases with temperature and reaches a value of 1.18 ms at room temperature (similar trends are reported in [19]). Fluorescence lifetime measurements performed with pinholes show that (Fig. 5 (b)), the measured increase in fluorescence lifetime with temperature is most likely due to the increased role of radiation trapping (due to the overlapping absorption and emission bands at elevated temperatures). As we can see from Fig. 5 (b), for the 1% Yb-doped sample, the intrinsic radiation trapping free lifetime of Yb:YAG is estimated to be around 1 ms both at 78 K and 300 K.

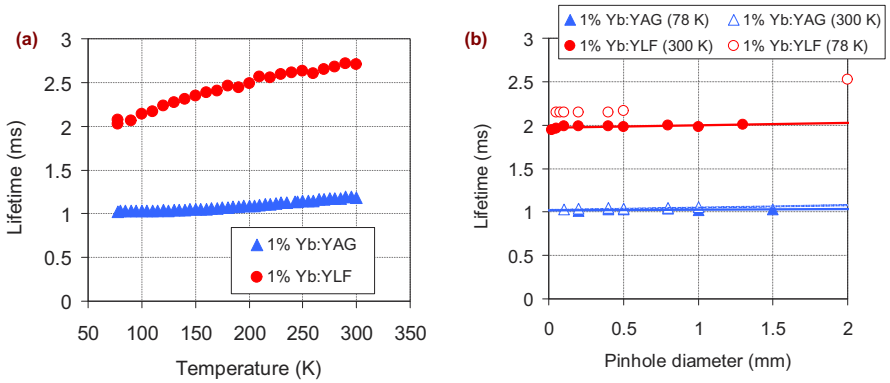

Fig. 5. (a) Measured variation of fluorescence lifetime of 1% Yb-doped Yb:YAG and Yb:YLF crystals in the 78-300 K range. (b) Measured variation of fluorescence lifetime with circular pinhole aperture diameter for 1% Yb-doped Yb:YAG and Yb:YLF samples at 78 K and 300 K. The reduced pinhole diameter minimizes radiation trapping effects, and could be used to estimate the intrinsic (radiation trapping free) fluorescence lifetime of the laser materials.

For the case of 1% Yb-doped YLF, we have measured a lifetime of 2.02 ms at 78 K, which again monotonically increases to 2.7 ms at room temperature. Due to the smaller crystal field strength of the YLF host (compared to YAG), the overlap of absorption and emission bands is stronger, and radiation trapping effect is more dominant in Yb:YLF. Hence, the increase of effective lifetime with temperature (from 2.02 ms to 2.8 ms) is larger compared to Yb:YAG (from 1.02 ms to 1.18 ms). By employing measurements with pinholes, we have estimated the radiation trapping free intrinsic lifetimes of Yb:YLF as 1.97 ms and 2.1 ms at 78 K and 300 K, respectively. These values are in relatively good agreement with literature [4,13,56,57,63]. We would like to note that, the estimated intrinsic lifetime at room-temperature (2.1 ms) is slightly higher than the intrinsic lifetime estimates at 78 K (1.97 ms). We believe that this difference might be due to the remaining radiation trapping effect that could not be eliminated fully. As another explanation, Püschel et al. proposed [56] that, this increase in estimated intrinsic fluorescence lifetime might be due to an increase in effective radiative lifetime with temperature (lifetime of the upper laser manifold changing due to variation of the Boltzmann occupation factors of the Stark sub-levels with temperature [64]). Overall, when we compare Yb:YLF and Yb:YAG in terms of their fluorescence lifetime, we see that Yb:YLF with its 2-fold longer lifetime could provide advantages in terms of inversion acquisition in the design of cryogenic amplifier systems.

Optical Materials EXPRESS

3.3. Comparison of emission spectra

The emission cross section (ECS) is one of the most important parameters in determining amplifier performance, and in this sub-section we will compare the ECS curves of cryogenic Yb:YAG and Yb:YLF in great detail. Figure 6 (a-c) presents the measured ECS spectra of Yb:YAG and Yb:YLF in the 78-200 K range. From our earlier work, we know that, under thermal load, the crystals in cryogenic systems easily reach temperatures of 125-150 K during regular laser/amplifier operation [29,53]. Hence, rather than comparing the emission spectra at 78 K, it is more beneficial to look at the spectra at slightly elevated temperatures. For that purpose, Fig. 6 (d) shows the measured emission cross section for Yb:YAG and Yb:YLF at 150 K. At 150 K, Yb:YAG has a peak emission cross section of 7.8 $\times 10^{-20}$ cm^2 at around 1029.5 nm, and the line had a FWHM of around 1.75 mm. This transition also has a rather sharp shape, and as earlier results have shown, upon strong gain narrowing, the obtainable pulses from cryogenic Yb:YAG systems are then only around 4-5 ps short [20–23].

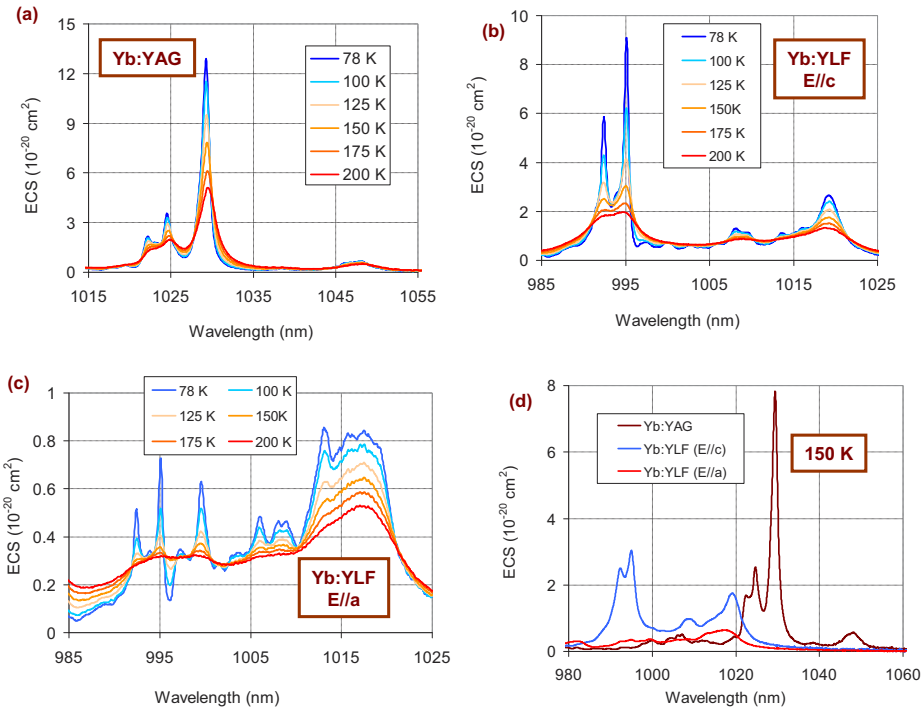

Fig. 6. Measured variation of (a) Yb:YAG, (b) Yb:YLF E//c axis and (c) Yb:YLF E//a axis emission cross section with temperature in the 78-200 K range. (d) Emission cross section of Yb:YAG and Yb:YLF at 150 K.

For comparison, the E//c axis of Yb:YLF has a peak ECS of 3.05×10^{-20} cm^2 centered around 995.1 nm with a FWHM of around 3 nm (extends to a width as wide as 5.5 nm if one considers the asymmetric shoulder towards the shorter wavelengths). As we can see, at 150 K, the 995.1 nm transition of Yb:YLF is around 2.5 times weaker compared to the 1029.5 nm transition of Yb:YAG. On the other hand, the 995.1 Yb:YLF peak is around 2 times wider, and in well-designed systems, it could potentially produce sub-2-ps level pulses [28].

Note that, the E//c axis of Yb:YLF has another line centered around 1019.3 nm with a peak ECS value of 1.8×10^{-20} cm^2 at 150 K, and this transition has a FWHM of around 8 nm, that could be used in generation/amplification of sub-500-fs level pulses [29]. More importantly, the E//a axis of Yb:YLF has a transition around 1017.5 nm with a peak ECS value of 0.65 $\times 10^{-20}$

Optical Materials EXPRESS

cm^2. The interesting part for this transition is, the emission curve around this transition is rather flat, which is quite beneficial in minimizing gain narrowing effect. Moreover, this transition has a FWHM of around 12 nm at 150 K, which could ideally support generation/amplification of sub-250-fs level pulses [25]. Hence, despite its lower emission cross section, due to its broad emission lines, especially in the E//a axis, the cryogenic Yb:YLF amplifier system has attracted a great deal of interest over the last decades [14,24,27–29,65,66]. On the other hand, compared to Yb:YAG, Yb:YLF systems have lower gain, and care must be taken in terms of optical losses for the design and implementation of efficient cryogenic Yb:YLF amplifiers.

In closing this sub-section, it is also beneficial to compare Yb:YAG and Yb:YLF systems in terms of emission saturation fluence parameter. The 1029.5 nm transition of Yb:YAG has a saturation fluence of around 2.5 J/cm^2 at 150 K. In comparison the saturation fluence of Yb:YLF is 6.55 J/cm^2 and 10.8 J/cm^2 for the 995.1 nm and 1019.3 nm transitions of E//c axis, and around 30 J/cm^2 for the 1017.5 nm transition of E//a axis, respectively. We want to point out that the saturation fluence for the broadband E//a axis transition of Yb:YLF around 1017.5 nm is even higher than the laser-induced damage threshold of standard optics (20 J/cm^2 for 10 ns pulses). As a result, the cryogenic Yb:YLF amplifiers are operated at much lower fluences than their saturation fluence [67], resulting in lower extraction efficiencies than in Yb:YAG amplifiers that can be operated at fluences close to their saturation fluence (2.5 J/cm^2). One way to improve the extraction efficiency of Yb:YLF systems is to operate them at high repetition rates (multi-kHz regime) and use the benefit of cumulative saturation effect of close by pulses. In this mode, Yb:YLF amplifiers could reach efficiencies close to 80% [29]. Moreover, high repetition rate operation of Yb:YLF amplifiers also enables better performance in terms of pulse-to-pulse energy stability.

3.4. Comparison of fractional thermal load

One of the crucial factors determining the power scalability of a laser system is the thermal conductivity of the laser material. The thermal conductivity of the YAG host is around 1.5 times higher than for the YLF host at cryogenic temperatures (e.g. 26.4 $Wm^{-1}K^{-1}$ in YAG versus 17.1 $Wm^{-1}K^{-1}$ for E//c axis of Yb:YLF at 150 K) [18]. Hence, the higher thermal conductivity of YAG provides an advantage in terms of thermal effects. On the other hand, one should also consider the thermal load on the crystal, and in a first order approximation the thermal load on the crystal scales with the quantum defect of the system (fractional thermal load might be 1.5×2 times higher than the quantum defect [5,53]).

For this purpose, in Fig. 7 (a) (right vertical axis), we show the calculated mean emission wavelength for Yb:YLF and Yb:YAG gain media as a function of temperature (calculations are performed by using the temperature-dependent emission data that is discussed earlier). As we can see form Fig. 7 (a), the mean emission wavelength in Yb:YLF is shorter than Yb:YAG at all temperatures due to the smaller crystal field strength of YLF host. As an example, at 150 K, the mean emission wavelength for Yb:YLF and Yb:YAG are 1000.45 nm and 1021.85 nm, respectively. Of course, these values might be different for different doping levels and gain media geometries due to the effect of radiation trapping, but the numbers given here are adequate for a first order estimation. Based on the calculated mean emission wavelength data, we have also estimated variation of quantum defect with temperature in Yb:YAG and Yb:YLF considering a pump wavelength of 940 nm for Yb:YAG and 960 nm for Yb:YLF (left vertical axis in Fig. 7 (a)). As one can see, due to the longer pump wavelength and shorter mean emission wavelength, Yb:YLF has a much lower quantum defect compared to Yb:YAG. Estimated quantum defect of Yb:YLF is around 4.05%, compared to 8% in Yb:YAG (under non-lasing conditions).

Overall, we see that, YAG host provides around 1.5 times higher thermal conductivity than YLF, but Yb:YLF has around ~2 times lower thermal load under the same absorbed pump power level. This shows that Yb:YLF is slightly better in terms of thermal heating of the

Optical Materials EXPRESS

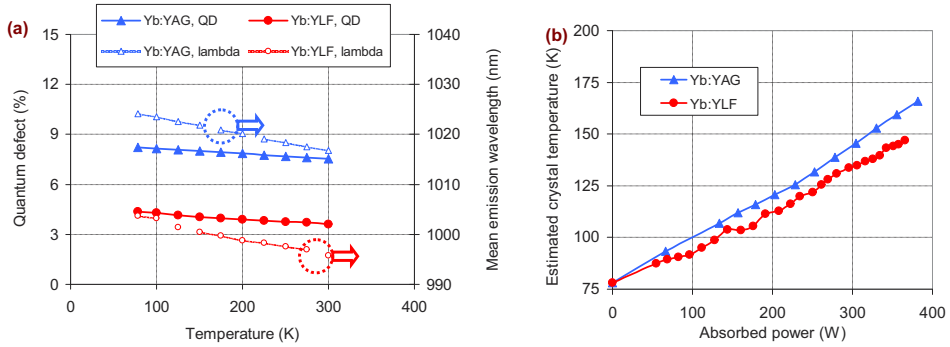

Fig. 7. (a) Calculated mean emission wavelength and quantum defect for Yb:YAG and Yb:YLF in non-lasing conditions, assuming pump wavelengths of 940 nm (Yb:YAG) and 960 nm (Yb:YLF). (b) Measured variation of estimated average crystal temperature with absorbed pump power level for Yb:YAG and Yb:YLF.

crystal when one only considers thermal conductivity and thermal load parameters (one expects around 25% lower temperatures in YLF host compared to YAG). Our direct measurements of crystal temperatures under almost identical conditions also confirmed this first order expectation. Figure 7 (b) shows the measured average temperatures of 1%Yb-doped Yb:YAG and Yb:YLF crystals as a function of absorbed pump power under non-lasing conditions in identical setups. We see that, for Yb:YAG the temperature of the crystal increases with a slope of around 0.23 K/W, whereas the slope in Yb:YLF is lower and is at 0.19 K/W (~20% lower slope). The analysis shows that in equally designed systems, the temperatures in Yb:YLF crystals could actually be lower than Yb:YAG despite its lower thermal conductivity. As a final note, the lasing wavelength of Yb:YAG (~1030 nm) is considerably higher than its mean emission wavelength (~1021.85 nm at 150 K), and hence while lasing the quantum defect in Yb:YAG is actually higher compared to its non-lasing condition. In comparison, in Yb:YLF, for the lasing wavelength of 995 nm, the quantum defect in lasing conditions is actually lower than in the non-lasing situation.

3.5. *Comparison of lasing performance in the short-cavity*

In the earlier sections, we have discussed the spectroscopic properties of Yb:YLF and Yb:YAG in a comparative manner, and presented pros and cons of each system. Starting from this sub-section, we will begin to compare the performance of the cryogenic Yb:YAG and Yb:YLF crystals in lasing experiments. During these experiments, we have just exchanged the dewars (containing either the Yb:YLF and Yb:YAG crystals) in the setup, and everything else was kept identical in the setups (except the pump wavelength). Hence, to the best of our knowledge the following data compares the performance of Yb:YAG and Yb:YLF in almost identical conditions.

In this sub-section, we will first compare the lasing performance for the short flat-flat laser cavity as described earlier (Fig. 2 (a)). Figure 8 summarizes the measured lasing performance of Yb:YAG and Yb:YLF for this configuration. All the data in Fig. 8 are taken using a 25% output coupler. In Fig. 8, we have also plotted the measured average temperature of the crystals at different pumping levels under lasing conditions. As we can see from Fig. 8 (a), in the short-cavity configuration, the Yb:YAG laser has a lasing threshold of 12.5 W, and initially it reaches a slope efficiency as high as 86%. At an absorbed pump power of 468 W (485 W incident, ~96.5% absorption), the Yb:YAG laser produces 365 W of output power at a 1030 nm wavelength. Note that the observed slope efficiency (86%) is rather close to the quantum defect limited performance (91.2%: considering 940 nm pumping and 1030 nm lasing). We see from Fig. 8 (a) that, at an absorbed pump power above 300 W, the performance of the system starts

Optical Materials EXPRESS

to degrade due to deleterious effect of thermal lensing, and beyond 480 W of absorbed pump power, the thermal lens becomes too dynamic to stabilize the laser, and the output power starts to decrease. Note that, at these pump power levels we have measured average crystal temperatures above 200 K. Also, part of the increase of crystal temperature is due to the retro-reflection of the unabsorbed pump light by the output coupler (hence measured temperatures are higher compared to non-lasing case: Fig. 7). Finally, the kink in the temperature estimation curve at around 250 W absorbed pump power is due to an effort for the realignment of the laser at that point, which proves the sensitivity of the employed temperature estimation method [53].

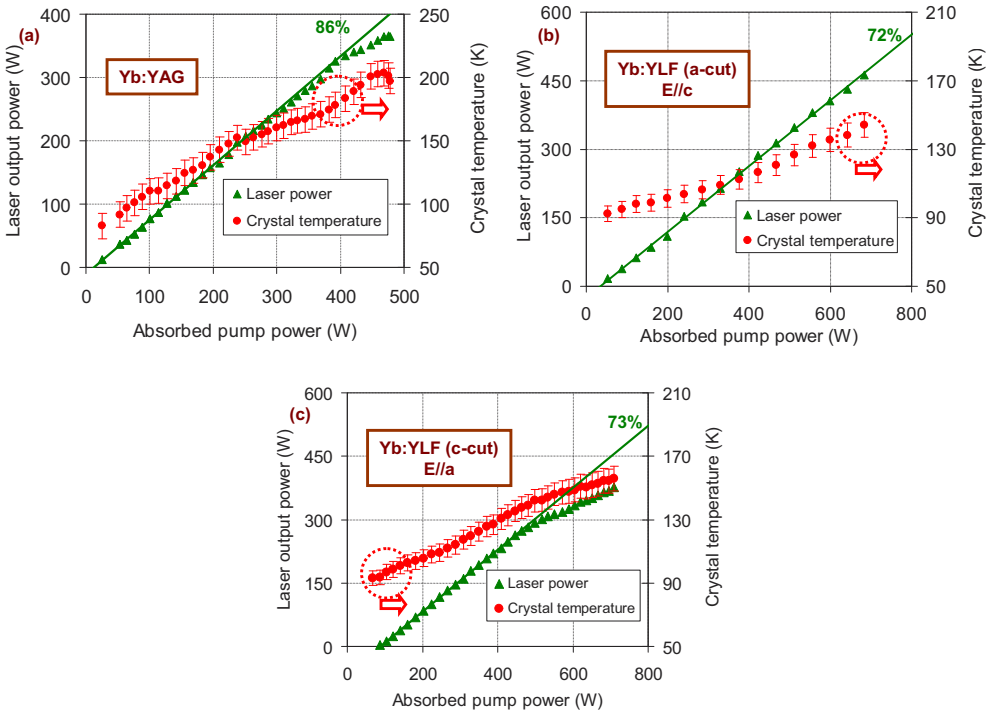

Fig. 8. Measured CW lasing efficiency for (a) Yb:YAG, (b) Yb:YLF in E//c axis and (c)Yb:YLF in E//a axis in short flat–flat cavity configuration using 25% output coupling. Variation of measured average crystal temperature with absorbed pump power level is also shown for all cases.

For comparison, by using the E//c axis of Yb:YLF (Fig. 8 (b)), we have measured a lasing threshold of around 35 W, and obtained a slope efficiency of 72%. We can partially explain the higher lasing threshold of Yb:YLF (35 W) compared to Yb:YAG (12.5 W) with the lower small signal gain coefficient (the gain product, the product of emission cross section and lifetime is around $8\,x10^{-23}$ cms in Yb:YAG versus $6\,x10^{-23}$ cms in Yb:YLF at 125 K). However, on top of that, we believe the stronger thermal lens in Yb:YAG also results in a smaller intracavity laser beam, which also reduces the lasing threshold. For the E//c axis of Yb:YLF, at an absorbed pump power of 683 W (710 W incident, ~96.2% absorption), the Yb:YLF E//c axis laser produced 462 W of output power at the wavelength of 1019 nm. At lower pump powers, the lasing wavelength is 995 nm (up to 50 W of output power), which then shifts to 1019 nm due to temperature induced changes in the gain spectrum (the wavelength transition point is output coupler dependent, since besides temperature, the gain spectra also depends on inversion [47,49]). It is interesting to see that, due to better thermal behavior of the Yb:YLF crystal, we could apply around 1.5 times higher pump power to the Yb:YLF crystal in comparison to the Yb:YAG, which enables extraction of

Optical Materials EXPRESS

higher output power levels (462 W in YLF host versus 365 W in YAG host). The measured average temperature of the Yb:YLF crystal is also lower compared to Yb:YAG due to reasons that have been discussed earlier.

Finally, using the E//a axis of Yb:YLF with the lower gain cross section (Fig. 8 (c)), we have measured a lasing threshold of around 85 W, and obtained an initial slope efficiency of 73%. At an absorbed pump power of 709 W (793 W incident, ~89.4% absorption), the E//a axis Yb:YLF laser produced 376 W of output power at 1018 nm wavelength. Note that, despite its lower gain, the performance obtained in E//a axis of Yb:YLF laser is still slightly better than Yb:YAG, but not as good as the performance observed with E//c axis of Yb:YLF due to the stronger thermal lensing observed while lasing in this axis (the anisotropic thermal lens behavior of YLF host will be discussed in greater detail in the upcoming sections).

3.6. Comparison of lasing performance in the long standing-wave cavity

In the previous section, we compared the laser performance of Yb:YAG and Yb:YLF in a short flat-flat cavity. In this section, we will compare their CW laser performance in a long standing-wave cavity (Fig. 2 (b)), that is more sensitive to thermal lensing of the gain element. Note that, this cavity resembles regenerative amplifier cavities we have employed with Yb:YLF earlier [29,60,66]. Hence the data presented here provides a better hint for regenerative amplification performance of these systems. The CW lasing performance of Yb:YLF and Yb:YAG in the long cavity configuration is summarized in Fig. 9. Again, this data is taken in the same cavity by just exchanging the laser crystals and pump module. In the case of Yb:YAG (Fig. 9 (a)), we have measured a lasing threshold of 12.5 W and an initial slope efficiency of 80% using 25% output coupling, a performance somewhat similar to the short-cavity case. On the other hand, due to the sensitivity of the longer cavity to thermal lensing, we could only apply incident pump power up to 217 W, and achieved a cw output power of 112 W from the system (absorbed power: 191 W, absorption:88%). At this pump power level, the average crystal temperature is measured to be just around 130 K, which shows that the limited performance is not due to the overheating of the crystal (as the Yb:YAG crystal in the short cavity reaches temperatures of 200 K). The main reason for limited performance is the strong thermal lensing created in the Yb:YAG rod that deteriorates the mode-matching between the cavity and pump modes, and destabilizes the cavity. The measured near-field beam profile of the Yb:YAG laser output (Fig. 9 (d)) also confirms the presence of a strong positive thermal lens. Note that the original beam with a dimeter of around 2 mm, shrinks down to a dimeter of 1.2 mm at 200 W absorbed pump power.

For comparison, while employing the E//c axis Yb:YLF crystal, we have measured a lasing threshold of 50W and a slope efficiency of 76% using a 40% transmitting output coupler (Fig. 9 (b)). Unlike, Yb:YAG, the thermal lens was rather weak, and we could apply incident pump power levels up to 840 W, and obtained an output power of 506 W at a wavelength of 1019 nm (absorbed power: 782 W, absorption: 93%, crystal temperature: 155 K). Due to the weak thermal lens, the performance obtained in the long standing wave cavity is similar to the short cavity for the case of E//c axis of Yb:YLF. The measured output beam profile near the OC (Fig. 9 (e)) also confirms that, the thermal lens is weak and oscillates between positive and negative values for horizontal and vertical directions.

Lastly, Fig. 9 (c) shows the laser performance of the long-standing cavity while employing the E//a axis of Yb:YLF. We have measured a lasing threshold of 55 W and a slope efficiency of 74% using a 25% transmitting output coupler. At an absorbed pump power of 717 W (843 W incident, ~85% absorption, crystal temperature: 178 K), the Yb:YLF E//a axis laser produced 325 W of output power at the wavelength of 1018 nm in the long standing-wave cavity. As can be seen from Fig. 9 (f), for the E//a axis, the TL is stronger than E//c axis of Yb:YLF, and this results in a faster deterioration of beam quality and bending of the CW efficiency curve. As a side note, compared to E//c axis, the crystal temperature is higher while using the E//a axis of Yb:YLF, and

Optical Materials EXPRESS

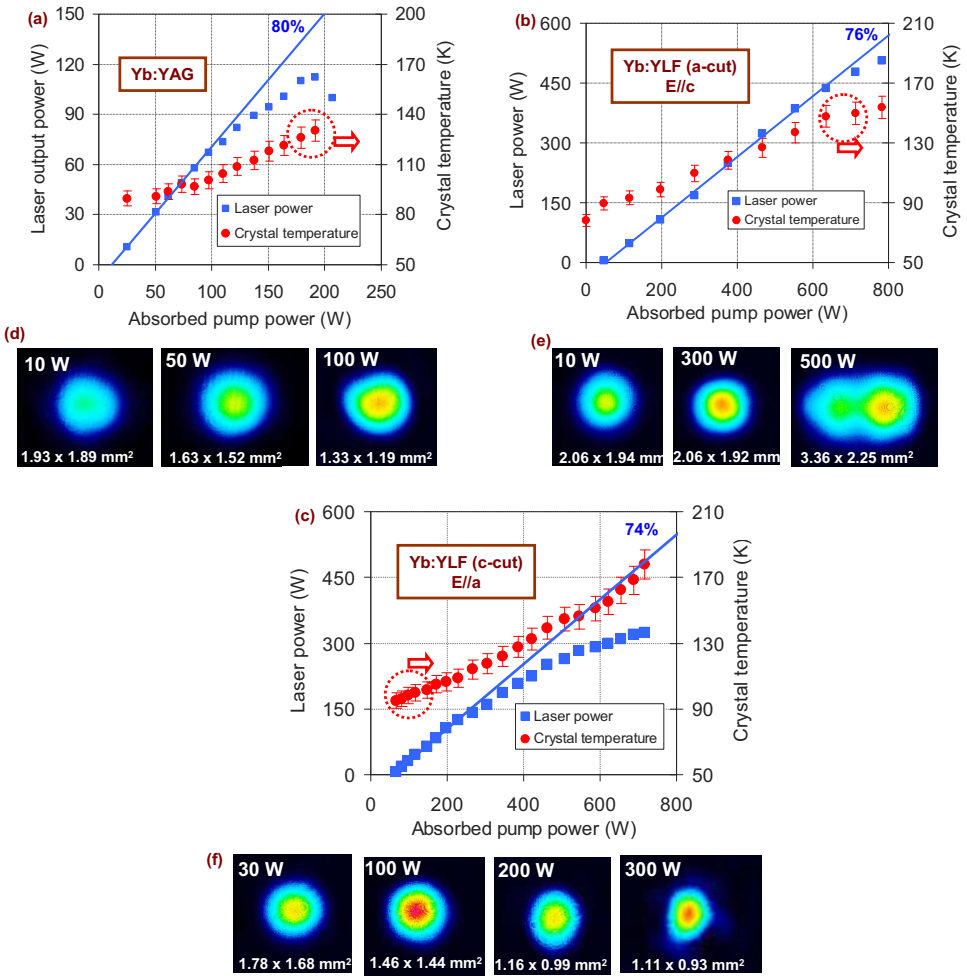

Fig. 9. Measured CW lasing efficiency of (a) Yb:YAG (b) Yb:YLF in E//c axis and (c)Yb:YLF in E//a axis in the long standing-wave cavity using 25% (a-c) and 40% (b) output couplers. Variation of measured average crystal temperature with absorbed pump power level is also shown for all cases. Representative near-field beam profiles of the long-cavity (d) Yb:YAG (e) Yb:YLF in E//c axis and (f)Yb:YLF in E//a axis lasers.

Optical Materials EXPRESS

some of these temperature increase is due to the inefficient extraction of the laser. As we can see from Fig. 9 (c), once the laser power curve starts to bend down due to the mode mismatch caused by the thermal lens, the slope of the measured crystal temperature starts to increase.

Overall, the laser experiments performed either in the short or long cavity configurations demonstrated that, Yb:YLF is more suitable for power scaling due to its weaker thermal lens. Especially, there is a significant performance difference while employing the long-standing wave cavity (506 W with YLF host versus 112 W with YAG), due to the sensitivity of the cavity to thermal lensing. Furthermore, a polarization dependent thermal lens is observed in Yb:YLF which provides an advantage to its E//c axis compared to the E//a axis in terms of power scalability (506 W with E//c axis versus 325 W with E//a axis).

3.7. Comparison of thermal lens strength

In the earlier sections, the experimental data on laser performance of Yb:YAG and Yb:YLF indicated that the thermal lens is rather weak especially in E//c axis of Yb:YLF, which provides a strong advantage in terms of power scaling. In order to confirm these results independently, we have also performed a direct measurement of the thermal lens strength. To start our discussion, Fig. 10 shows the recorded variation of the beam shape of a transmitted probe beam at 1064 nm at different levels of absorbed pump power. In the experiments, the collimated beam passes through the dewar containing the Yb:YAG/Yb:YLF crystals and is monitored 1 m after crystal for Yb:YAG and 2 m after the crystal for the case of Yb:YLF (a shorter distance is used in the case of Yb:YAG due to the stronger thermal lensing). Hence, the 1064 nm beam probes the status of the thermal lens of the crystals while the system is pumped with the high power diode modules, and provides us direct information on the thermal lens.

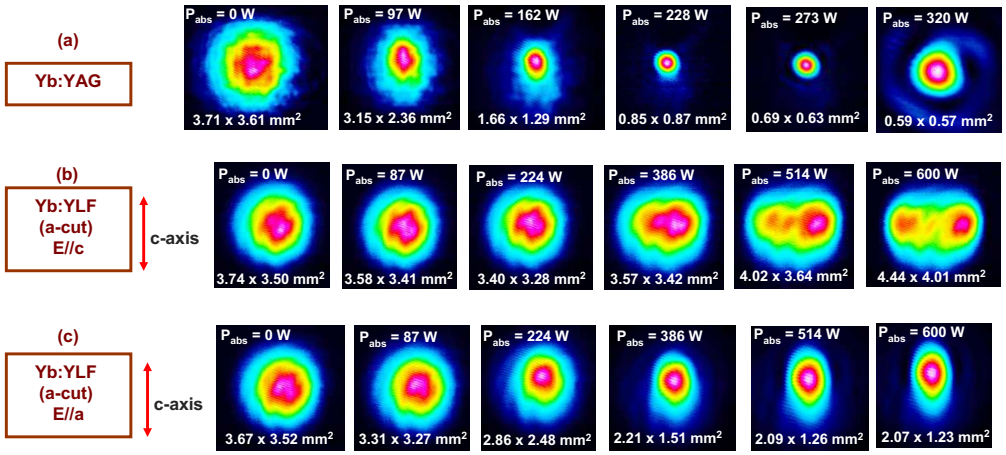

Fig. 10. Measured variation of the transmitted 1064 nm probe beam profile as a function of absorbed pump power for (a) Yb:YAG, (b) Yb:YLF E//c axis configuration, and (c) Yb:YLF E//a axis configuration.

First of all, note that the behavior of the beam shape at different absorbed pump power levels are in accordance with the measured near-field beam profile data in the long cavity cw laser experiments (Fig. 9 (d-f)). As an example, for the E//c axis of Yb:YLF, the beam size does not change much in the vertical direction and elongates in the horizontal direction as we see both from Fig. 9 (e) and Fig. 10 (b). As a side note, the behavior of the beam is also similar to what we have observed earlier in the regenerative amplifier studies performed using E//c [29] and E//a axis configuration [60,66] of Yb:YLF. As the next step, using the measured beam profile data and simple ABCD matrix formalism, we have calculated the thermal lens strength in Yb:YAG

Optical Materials EXPRESS

and Yb:YLF crystals and the data is summarized in Fig. 11. Figure 11 also includes thermal lens strength estimation using the long-cavity near-field beam profile data, which is denoted as cavity in the figure legends. Furthermore, some of the data is repeated a few times for confirmation.

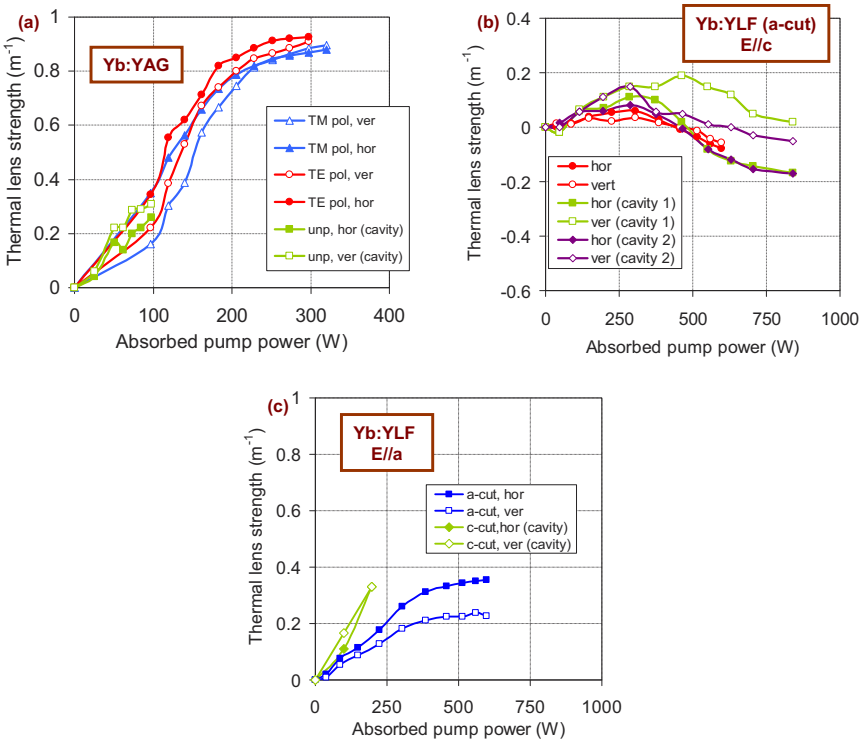

Fig. 11. Estimated thermal length strength of (a) Yb:YAG (b) Yb:YLF in E//c axis and (c)Yb:YLF in E//a axis using direct thermal lens measurements as well as estimation from measured cavity beam size after the output coupler in standing-wave cavity. Some of the data is repeated a few times for confirmation of the results.

In the case of Yb:YAG (Fig. 11 (a)), we see that the thermal lens is positive and rather strong and reaches a value of around ~1.1 m (~0.9 m^{-1} diopters) at an absorbed pump power of only 300 W (crystal temperature: ~145 K, Fig. 7(b)). The thermal lens estimated from the long cw lasing cavity data matches the direct measurements quite well, confirming the accuracy of the measurements. Moreover, there is no significant difference for different incident probe beam polarizations and for the different directions of the beam (vertical and horizontal) as expected from the isotropic crystal structure of YAG. This also shows that, to first order, the asymmetric cooling of the crystals (from their top side) does not create a significant asymmetry in thermal lens behavior: more sensitive measurement with wave-front sensors is required to resolve the higher-order effects of asymmetric cooling.

When we look at the thermal lens behavior in E//c axis of Yb:YLF (Fig. 11 (b)), we see that the thermal lens is much weaker and oscillates between ± 5 meters (±0.2 m^{-1} diopters). We believe that, this oscillation of thermal lens strength and sign is due to temperature dependence of the strength of thermal lens coming from different mechanisms (as an example the thermo-optic coefficient of Yb:YLF increases with temperature [18]). There is some fluctuation in the experimental data, but one can also see that, at the absorbed pump power of 850 W, the thermal lens strength is rather small and very close to zero (-0.05 m^{-1} to 0.02 m^{-1} diopters) in the vertical axis (parallel to the c axis direction for this a-cut crystal). For the horizontal axis, the thermal

Optical Materials EXPRESS

lens is negative and a little stronger, and reaches a value of minus 5-6 meters (-0.2 m^{-1} diopters), which creates the observed asymmetry in the beam profile. Similar to the Yb:YAG case, the thermal lens estimated from the long cw lasing cavity data and earlier regenerative amplifier studies [29] matches the direct measurements relatively well.

Finally, for the E//a axis of Yb:YLF (Fig. 11 (c)), we see that the thermal lens is positive and stronger compared to E//c axis. At an absorbed pump power of 600 W, we have estimated a thermal lens of 3 m (0.35 m^{-1} diopters) and 4.5 m (0.22 m^{-1} diopters) for the horizontal and vertical directions, respectively. Note that, the E//a axis of Yb:YLF could be explored using either a-cut and c-cut crystals. A slightly better performance is observed with the a-cut sample, which might be due to the more efficient cooling of the sample via the c-axis which has higher thermal conductivity (in identical conditions, crystal in Fig. 1. (a) will cool better than the crystal in Fig. 1 (b), as the c-axis with higher conductivity is employed for cooling). Finally, for the E//a axis, the thermal lens behavior in the long cw lasing cavity and earlier regenerative [60,66] and multi-pass amplifier [65,68] studies are also in accordance with direct measurements.

To our knowledge, literature lacks detailed information on thermal lens behavior of Yb:YLF, especially for systems operating at cryogenic temperatures. On the other hand, thermal lensing has been studied at room-temperature in other YLF systems doped with laser active ions of Nd and Tm [69–71]. Looking at the literature on Nd:YLF, which also provides lasing in a similar wavelength range, we see that an asymmetric/anisotropic and weak thermal lens is also observed in many studies confirming the finding in this study [32–39]: a negative thermal lens while employing E//c axis, and a positive thermal lens while using E//a axis. Hence, we see that, the thermal lens observations in cryogenic Yb:YLF systems made here, are in good agreement with the room-temperature Nd:YLF systems [32–39].

It is also interesting to understand the origin of the thermal lens asymmetry observed in Yb:YLF (or similarly in earlier Nd:YLF systems). As also underlined by Zhang et al. [35], due to the biaxial anisotropy of the YLF crystal, many of the parameters of Yb:YLF including thermal conductivity, thermo-optical coefficient, thermal expansion coefficient are different for a and c axes [18], which leads to the observed asymmetry. For our specific case, asymmetric and one sided cryogenic cooling of the samples might also play a role (which we believe to be minor).

Several mechanisms contribute to the overall thermal lensing of a laser crystal, including: (i) the change of optical path due to change in refractive index with temperature, (ii) bulging of the end faces of the rod due to thermal expansion, (iii) thermally induced mechanical stress generating changes in refractive index (lensing due to photoelastic effect) and (iv) population inversion induced changes in refractive index (also known as electronic lensing). The thermal coefficient of the refractive index (dn/dT, thermo-optic coefficient) is reported to be negative for both axes of YLF [18,72,73]. For the c-axis, the dn/dT parameter of YLF has a larger reported value compared to that of the a-axis (-2.5 ppm/K in c-axis versus -1 ppm/K in a-axis, at 150 K [18]). Hence, the thermal lens induced by the thermo-optic effect will be negative and will be larger while employing the E//c axis for lasing. Other contributions to thermal lensing, e.g. due to surface bulging and photoelastic effect with a positive sign, then partially balance or even overcompensate the negative thermal lens induced by the thermo-optic effect [67] (as an example see Table 2 in [35]). To our knowledge, the contribution of thermal lensing due to population/electronic lensing is not yet known for Yb:YLF, as the polarizability difference parameter (α) has so far not been measured [74].

In earlier reports with Nd:YLF, stress-induced birefringence is assumed to be small [32], and Pollnau et al. explained the anisotropy in thermal lens performance with the difference in surface bulging induced by the asymmetric pump beam profile. Note that, for our case, the surface bulging contribution is expected to be small due to the usage of undoped YLF/YAG caps on crystal surfaces [67]. Moreover, due to the symmetric pump profile used, we do not have a pump induced asymmetry in surface-bulging induced lensing: only a small asymmetry will be

Optical Materials EXPRESS

present due to one sided cooling [67]. Hence, for the current study, surface-bulging should have a little role for the asymmetry observed in thermal lensing. Later reports of thermal lensing in Nd:YLF have shown that stress-induced changes in refractive index could be significant [35,38] in YLF, and could explain the asymmetry observed in thermal lensing quite well. We believe that, as in the case of Nd:YLF [35,38], for our cryogenic Yb:YLF system, stress-induced changes in refractive index are probably the main cause of the asymmetry observed in thermal lensing. Overall, additional detailed experiments should be performed for a better understanding of the thermal-lensing behavior observed in cryogenic Yb:YLF laser and amplifier systems.

4. Conclusions

We have presented detailed spectroscopic, temperature, lasing and thermal-lens measurements made with almost identical Yb:YLF and Yb:YAG systems at cryogenic temperatures, and based on these experimental data, we have discussed pros and cons of each system from many perspectives. Table 1 lists the main parameters of Yb:YAG and Yb:YLF that is discussed throughout this text and provides a brief summary.

Table 1. Comparison of thermal, mechanical and optical parameters of Yb:YLF and Yb:YAG for cryogenic lasing/amplification. Unless specified implicitly, the reported values are those measured at 150 K for un-doped samples

Gain Medium	Yb:$LiYF_4$ (Yb:YLF)	Yb^{+3}:$Y_3Al_5O_{12}$ (Yb:YAG)
Fracture toughness [x10^6 Pa $m^{1/2}$]	0.27 [75]	1.4 [75]
Thermal conductivity [W/K.m]	12.4 (//a), 17.1 (//c) [18]	26.4 [18]
Thermal expansion coefficient [x10^{-6}/K]	5.68 (//a), 5.51 (//c) @ 140 K [18]	3.15 @ 140 K [18]
Temperature dependence of refractive index [x10^{-6} K]	-1 (//a), -2.5 (//c) [18]	3 [18]
Suitable pumping wavelength [nm]	960	940
Peak absorption cross section [x10^{-20} cm^2]	2.5(//a), 5.6 (//c) @ 78 K	1.4 @ 78 K
Absorption saturation intensity [kW/cm^2]	4.2(//a), 1.85 (//c) @ 78 K	15.1 @ 78 K
Laser/amplification central wavelength [nm]	1017.5 (//a), 995.1 and 1019.3 (//c)	1029.5
Peak emission cross section [x10^{-20} cm^2]	0.65 (//a), 3.05 and 1.8 (//c)	7.8
Laser/amplification bandwidth [nm]	12 (//a), 3 and 8 (//c)	1.75
Quantum Defect (%)	5.7(//a), 3.5 and 5.8 (//c)	8.7
Fluorescence lifetime [ms]	2	1
Gain product [x10^{-23} cm^2s]	1.3 (//a), 6.1 and 3.6 (//c)	7.8
Gain saturation fluence [J/cm^2]	30 (//a), 6.6 and 10.8 (//c)	2.5

In terms of absorption, neither Yb:YLF nor Yb:YAG could be pumped efficiently at their zero phonon wavelength (~970 nm) at cryogenic temperatures, as the current state-of-the-art high power diode modules have an emission bandwidth much broader than the absorption bandwidth of these lines. As a result, cryogenic Yb:YLF systems are usually pumped at 960 nm, and compared to the Yb:YAG systems that are pumped at 940 nm, this provides YLF host an advantage in terms of quantum defect. Moreover, the mean emission wavelength of Yb:YLF is located at a shorter wavelength compared to Yb:YAG, which also lowers the quantum defect of the crystal. Overall, despite the higher conductivity the YAG host, the temperature increase of the Yb:YLF crystals

Optical Materials EXPRESS

under similar pumping conditions is lower than to Yb:YAG in otherwise identically designed systems.

In terms of emission cross section, Yb:YAG provides a stronger emission band than Yb:YLF (2-4 fold stronger than E//c axis and 10 fold stronger than the E//a axis). On the other hand, the emission bands are much wider in Yb:YLF, and especially the E//a axis emission located around 1017.5 nm has the potential to achieve sub-250-fs level pulses. Moreover, the fluorescence lifetime is about twice as long in Yb:YLF compared to Yb:YAG, which partially balances out its lower ECS compared to Yb:YAG. The thermal lens is also much weaker in Yb:YLF, especially while lasing in the E//c configuration, which enables pumping at higher intensities, which increases attainable gain levels and provides great advantage to Yb:YLF in terms of power scaling. Direct lasing performance measurements performed in identical cavities further confirmed the advantage of the YLF host. Especially in the long standing wave-cavity, where one is more sensitive to thermal lensing, we have achieved up to 506 W of output power while using the E//c axis configuration of Yb:YLF. In comparison, the Yb:YAG laser produced only up to 112 W under identical conditions.

Funding. Deutsche Forschungsgemeinschaft (390715994); Seventh Framework Programme (609920).

Acknowledgements. The authors acknowledge support from previous group members L. E. Zapata, K. Zapata for establishing the indium-bonding technology for YLF at CFEL-DESY. UD acknowledges support from BAGEP Award of the Bilim Akademisi.

Disclosures. The authors declare no conflicts of interest.

Data Availability. Data underlying the results presented in this paper are not publicly available at this time but may be obtained from the authors upon reasonable request.

References

1. H. Fattahi, H. G. Barros, M. Gorjan, T. Nubbemeyer, B. Alsaif, C. Y. Teisset, M. Schultze, S. Prinz, M. Haefner, M. Ueffing, A. Alismail, L. Vamos, A. Schwarz, O. Pronin, J. Brons, X. T. Geng, G. Arisholm, M. Ciappina, V. S. Yakovlev, D. E. Kim, A. M. Azzeer, N. Karpowicz, D. Sutter, Z. Major, T. Metzger, and F. Krausz, "Third-generation femtosecond technology," Optica **1**(1), 45–63 (2014).
2. C. Honninger, R. Paschotta, M. Graf, F. Morier-Genoud, G. Zhang, M. Moser, S. Biswal, J. Nees, A. Braun, G. A. Mourou, I. Johannsen, A. Giesen, W. Seeber, and U. Keller, "Ultrafast ytterbium-doped bulk lasers and laser amplifiers," Appl. Phys. B: Lasers Opt. **69**(1), 3–17 (1999).
3. P. Lacovara, H. K. Choi, C. A. Wang, R. L. Aggarwal, and T. Y. Fan, "Room-temperature diode-pumped Yb:YAG laser," Opt. Lett. **16**(14), 1089–1091 (1991).
4. L. D. DeLoach, S. A. Payne, L. L. Chase, L. K. Smith, W. L. Kway, and W. F. Krupke, "Evaluation of absorption and emission properties of Yb^{3+} doped crystals for laser applications," IEEE J. Quantum Electron. **29**(4), 1179–1191 (1993).
5. T. Y. Fan, "Heat generation in Nd:YAG and Yb:YAG," IEEE J. Quantum Electron. **29**(6), 1457–1459 (1993).
6. H. Bruesselbach and D. S. Sumida, "A 2.65-kW Yb: YAG single-rod laser," IEEE J. Sel. Top. Quantum Electron. **11**(3), 600–603 (2005).
7. M. Li, T. Zhou, L. Xu, Q. Gao, H. Hu, Y. Wu, D. Wang, J. Li, J. Lei, W. Lv, Y. Yu, Z. Wu, and N. Zhao, "High power continuous wave Yb:YAG composite crystal zigzag slab amplifier at room temperature," IEEE Photonics J. **9**(6), 1 (2017).
8. X. Délen, S. Piehler, J. Didierjean, N. Aubry, A. Voss, M. A. Ahmed, T. Graf, F. Balembois, and P. Georges, "250 W single-crystal fiber Yb:YAG laser," Opt. Lett. **37**(14), 2898 (2012).
9. A. Giesen and J. Speiser, "Fifteen years of work on thin-disk lasers: results and scaling laws," IEEE J. Select. Topics Quantum Electron. **13**(3), 598–609 (2007).
10. T. Dietz, M. Jenne, D. Bauer, M. Scharun, D. Sutter, and A. Killi, "Ultrafast thin-disk multi-pass amplifier system providing 1.9 kW of average output power and pulse energies in the 10 mJ range at 1 ps of pulse duration for glass-cleaving applications," Opt. Express **28**(8), 11415–11423 (2020).
11. J.-P. Negel, A. Loescher, A. Voss, D. Bauer, D. Sutter, A. Killi, M. A. Ahmed, and T. Graf, "Ultrafast thin-disk multipass laser amplifier delivering 14 kW (47 mJ, 1030 nm) average power converted to 820 W at 515 nm and 234 W at 343 nm," Opt. Express **23**(16), 21064 (2015).
12. T. Nubbemeyer, M. Kaumanns, M. Ueffing, M. Gorjan, A. Alismail, H. Fattahi, J. Brons, O. Pronin, H. G. Barros, Z. Major, T. Metzger, D. Sutter, and F. Krausz, "1 kW, 200 mJ picosecond thin-disk laser system," Opt. Lett. **42**(7), 1381–1384 (2017).
13. T. Y. Fan, D. J. Ripin, R. L. Aggarwal, J. R. Ochoa, B. Chann, M. Tilleman, and J. Spitzberg, "Cryogenic Yb^{3+}-doped solid-state lasers," IEEE J. Select. Topics Quantum Electron. **13**(3), 448–459 (2007).

Optical Materials EXPRESS

14. D. Rand, D. Miller, D. J. Ripin, and T. Y. Fan, "Cryogenic Yb3+-doped materials for pulsed solid-state laser applications [Invited]," Opt. Mater. Express **1**(3), 434–450 (2011).
15. D. C. Brown, "The promise of cryogenic solid-state lasers," IEEE J. Select. Topics Quantum Electron. **11**(3), 587–599 (2005).
16. D. J. Ripin, J. R. Ochoa, R. L. Aggarwal, and T. Y. Fan, "165-W cryogenically cooled Yb:YAG laser," Opt. Lett. **29**(18), 2154 (2004).
17. D. J. Ripin, J. R. Ochoa, R. L. Aggarwal, and T. Y. Fan, "300-W cryogenically cooled Yb:YAG laser," IEEE J. Quantum Electron. **41**(10), 1274–1277 (2005).
18. R. L. Aggarwal, D. J. Ripin, J. R. Ochoa, and T. Y. Fan, "Measurement of thermo-optic properties of $Y_3Al_5O_{12}$, $Lu_3Al_5O_{12}$, $YAlO_3$, $LiYF_4$, $LiLuF_4$, BaY_2F_8, $KGd(WO_4)_2$, and $KY(WO_4)_2$ laser crystals in the 80-300 K temperature range," J. Appl. Phys. **98**(10), 103514 (2005).
19. J. Dong, M. Bass, Y. Mao, P. Deng, and F. Gan, "Dependence of the Yb^{3+} emission cross section and lifetime on temperature and concentration in yttrium aluminum garnet," JOSA B **20**(9), 1975–1979 (2003).
20. B. A. Reagan, C. Baumgarten, E. Jankowska, H. Chi, H. Bravo, K. Dehne, M. Pedicone, L. Yin, H. Wang, C. S. Menoni, and J. J. Rocca, "Scaling diode-pumped, high energy picosecond lasers to kilowatt average powers," High Power Laser Sci. Eng. **6**, e11 (2018).
21. C. Baumgarten, M. Pedicone, H. Bravo, H. Wang, L. Yin, C. S. Menoni, J. J. Rocca, and B. A. Reagan, "1 J, 05 kHz repetition rate picosecond laser," Opt. Lett. **41**(14), 3339 (2016).
22. M. Pergament, L. E. Zapata, U. Demirbas, Y. Liu, M. Kellert, S. Reuter, J. Thesinga, Y. Hua, H. Cankaya, A.-L. Calendron, and F. X. Kärtner, "High energy cryogenic Yb:YAG and Yb:YLF chirped pulse amplifiers," in *Laser Congress 2020 (ASSL, LAC) (2020), Paper ATu4A.3* (The Optical Society, 2021), p. ATu4A.3.
23. L. E. Zapata, H. Lin, A. L. Calendron, H. Cankaya, M. Hemmer, F. Reichert, W. R. Huang, E. Granados, K. H. Hong, and F. X. Kärtner, "Cryogenic Yb:YAG composite-thin-disk for high energy and average power amplifiers," Opt. Lett. **40**(11), 2610–2613 (2015).
24. J. Kawanaka, K. Yamakawa, H. Nishioka, and K. Ueda, "30-mJ, diode-pumped, chirped-pulse Yb : YLF regenerative amplifier," Opt. Lett. **28**(21), 2121–2123 (2003).
25. J. Kawanaka, S. Tokita, H. Nishioka, M. Fujita, K. Yamakawa, K. Ueda, and Y. Izawa, "Dramatically improved laser characteristics of diode-pumped Yb-doped materials at low temperature," Laser Phys. **15**(9), 1306–1312 (2005).
26. L. E. Zapata, D. J. Ripin, and T. Y. Fan, "Power scaling of cryogenic Yb:$LiYF_4$ lasers," Opt. Lett. **35**(11), 1854–1856 (2010).
27. D. E. Miller, L. E. Zapata, D. J. Ripin, and T. Y. Fan, "Sub-picosecond pulses at 100 W average power from a Yb:YLF chirped-pulse amplification system," Opt. Lett. **37**(13), 2700–2702 (2012).
28. J. Manni, D. Harris, and T. Y. Fan, "High-gain (43 dB), high-power (40 W), highly efficient multipass amplifier at 995 nm in Yb:$LiYF_4$," Opt. Commun. **417**, 54–56 (2018).
29. U. Demirbas, M. Kellert, J. Thesinga, Y. Hua, S. Reuter, M. Pergament, and F. X. Kärtner, "Highly efficient cryogenic Yb:YLF regenerative amplifier with 250 W average power," Opt. Lett. **46**(16), 3865–3868 (2021).
30. U. Demirbas, J. Thesinga, M. Kellert, S. Reuter, M. Pergamnet, and F. X. Kärtner, "Semiconductor saturable absorber mirror mode-locked Yb:YLF laser with pulses of 40 fs," Opt. Lett. **47**(4), 933–936 (2022).
31. U. Demirbas, J. Thesinga, M. Kellert, S. Reuter, M. Pergament, and F. X. Kärtner, "Broadly tunable (993–1110 nm) Yb:YLF laser," Appl. Opt. **61**(13), 3702–3710 (2022).
32. M. Pollnau, P. Hardman, M. Kern, W. Clarkson, and D. Hanna, "Upconversion-induced heat generation and thermal lensing in Nd:YLF and Nd:YAG," Phys. Rev. B **58**(24), 16076–16092 (1998).
33. S. Merazzi, R. Gruber, and H. P. Weber, "Thermal beam distortions in end-pumped Nd: YAG, Nd:GSGG, and Nd:YLF rods," IEEE J. Quantum Electron. **30**(7), 1605–1615 (1994).
34. J. E. Murray, "Pulsed gain and thermal lensing of Nd:$LiYF_4$," IEEE J. Quantum Electron. **19**(4), 488–491 (1983).
35. Z. Zhang, Q. Liu, M. Nie, E. Ji, and M. Gong, "Experimental and theoretical study of the weak and asymmetrical thermal lens effect of Nd:YLF crystal for σ and π polarizations," Appl. Phys. B **120**(4), 689–696 (2015).
36. P. J. Hardman, W. A. Clarkson, G. J. Friel, M. Pollnau, and D. C. Hanna, "Energy-transfer upconversion and thermal lensing in high-power end-pumped Nd: YLF laser crystals," IEEE J. Quantum Electron. **35**(4), 647–655 (1999).
37. H. Vanherzeele, "Thermal lensing measurement and compensation in a continuous-wave mode-locked Nd:YLF laser," Opt. Lett. **13**(5), 369–371 (1988).
38. V. V. Zelenogorskii and E. A. Khazanov, "Influence of the photoelastic effect on the thermal lensin a YLF crystal," Quantum Electron. **40**(1), 40–44 (2010).
39. C.-W. Chen, C.-Y. Cho, H.-C. Liang, Y.-H. Fang, H.-C. Liang, and H.-C. Liang, "Investigation of anisotropic thermal lens effect in a dual-polarized Nd:YLF laser," Opt. Lett. **46**(1), 94–97 (2021).
40. N. U. Wetter and A. M. Deana, "Power scaling of a side-pumped Nd:YLF laser based on DBMC technology," Appl. Phys. B **117**(3), 855–860 (2014).
41. V. Bagnoud, M. J. Guardalben, J. Puth, J. D. Zuegel, T. Mooney, and P. Dumas, "High-energy, high-average-power laser with Nd:YLF rods corrected bymagnetorheological finishing," Appl. Opt. **44**(2), 282–288 (2005).
42. K. Scholle, S. Lamrini, F. Gatzemeier, P. Koopmann, and P. Fuhrberg, "In-band diode pumped high power Ho:YLF laser," 2013 Conf. Lasers Electro-Optics Eur. Int. Quantum Electron. Conf. CLEO/Europe-IQEC 2013 (2013).
43. Y. Kalisky, J. Kagan, H. Lotem, and D. Sagie, "Continuous wave operation of multiply doped Ho:YLF and Ho:YAG laser," Opt. Commun. **65**(5), 359–363 (1988).

Optical Materials EXPRESS

44. H. Tanaka, S. Fujita, and F. Kannari, "High-power visibly emitting Pr3+:YLF laser end pumped by single-emitter or fiber-coupled GaN blue laser diodes," Appl. Opt. **57**(21), 5923–5928 (2018).
45. S. So, J. I. MacKenzie, D. P. Shepherd, W. A. Clarkson, J. G. Betterton, and E. K. Gorton, "A power-scaling strategy for longitudinally diode-pumped Tm:YLF lasers," Appl. Phys. B **84**(3), 389–393 (2006).
46. T. M. Baer, D. F. Head, P. Gooding, G. J. Kintz, and S. Hutchison, "Performance of diode-pumped Nd: YAG and Nd: YLF lasers in a tightly folded resonator configuration," IEEE J. Quantum Electron. **28**(4), 1131–1138 (1992).
47. M. Kellert, U. Demirbas, J. Thesinga, S. Reuter, M. Pergament, and F. X. Kärtner, "High power (>500W) cryogenically cooled Yb:YLF cw-oscillator operating at 995 nm and 1019 nm using E/c axis for lasing," Opt. Express **29**(8), 11674 (2021).
48. U. Demirbas, H. Cankaya, J. Thesinga, F. X. Kärtner, and M. Pergament, "Efficient, diode-pumped, high-power (>300W) cryogenic Yb:YLF laser with broad-tunability (995-1020.5 nm): Investigation of E//a-axis for lasing," Opt. Express **27**(25), 36562 (2019).
49. U. Demirbas, J. Thesinga, M. Kellert, F. X. Kärtner, and M. Pergament, "Detailed investigation of absorption, emission and gain in Yb:YLF in the 78–300 K range," Opt. Mater. Express **11**(2), 250 (2021).
50. U. Demirbas, J. Thesinga, M. Kellert, M. Pergament, and F. X. Kärtner, "Temperature and doping dependence of fluorescence lifetime in Yb:YLF (role of impurities)," Optical Materials **112**, 110792 (2021).
51. U. Demirbas, "Cr:Colquiriite lasers: current status and challenges for further progress," Prog. Quantum Electron. **68**, 100227 (2019).
52. U. Demirbas, J. Thesinga, M. Kellert, F. X. Kärtner, and M. Pergament, "Comparison of different in situ optical temperature probing techniques for cryogenic Yb:YLF," Opt. Mater. Express **10**(12), 3403–3413 (2020).
53. U. Demirbas, J. Thesinga, M. Kellert, S. Reuter, F. X. Kärtner, and M. Pergament, "Error analysis of contactless optical temperature probing methods for cryogenic Yb:YAG," Appl. Phys. B **127**(8), 112 (2021).
54. D. C. Brown, R. L. Cone, Y. C. Sun, and R. W. Equall, "Yb : YAG absorption at ambient and cryogenic temperatures," IEEE J. Select. Topics Quantum Electron. **11**(3), 604–612 (2005).
55. J. Körner, V. Jambunathan, J. Hein, R. Seifert, M. Loeser, M. Siebold, U. Schramm, P. Sikocinski, A. Lucianetti, T. Mocek, and M. C. Kaluza, "Spectroscopic characterization of Yb^{3+}-doped laser materials at cryogenic temperatures," Appl. Phys. B **116**(1), 75–81 (2014).
56. S. Püschel, S. Kalusniak, C. Kränkel, and H. Tanaka, "Temperature-dependent radiative lifetime of Yb:YLF: refined cross sections and potential for laser cooling," Opt. Express **29**(7), 11106 (2021).
57. J. Korner, M. Kruger, J. Reiter, A. Munzer, J. Hein, and M. C. Kaluza, "Temperature dependent spectroscopic study of Yb^{3+}-doped $KG(WO_4)_2$, $KY(WO_4)_2$, $YAlO_3$ and $YLiF_4$ for laser applications," Opt. Mater. Express **10**(10), 2425–2438 (2020).
58. M. Smrz, T. Miura, M. Chyla, S. Nagisetty, O. Novak, A. Endo, and T. Mocek, "Suppression of nonlinear phonon relaxation in Yb:YAG thin disk via zero phonon line pumping," Opt. Lett. **39**(16), 4919–4922 (2014).
59. M. De Vido, A. Wojtusiak, and K. Ertel, "High-resolution absorption measurement at the zero phonon line of Yb:YAG between 80 K and 300 K," Opt. Mater. Express **10**(3), 717 (2020).
60. U. Demirbas, M. Kellert, J. Thesinga, Y. Hua, S. Reuter, F. X. Kärtner, and M. Pergament, "Comparative investigation of lasing and amplification performance in cryogenic Yb:YLF systems," Appl. Phys. B **127**(3), 46 (2021).
61. V. Jambunathan, T. Miura, L. Těsnohlídková, A. Lucianetti, and T. Mocek, "Efficient laser performance of a cryogenic Yb:YAG laser pumped by fiber coupled 940 and 969 nm laser diodes," Laser Phys. Lett. **12**(1), 015002 (2015).
62. H. Cankaya, U. Demirbas, A. K. Erdamar, and A. Sennaroglu, "Absorption saturation analysis of Cr^{2+}: ZnSe and Fe^{2+}: ZnSe," J. Opt. Soc. Am. B **25**(5), 794–800 (2008).
63. G. Brasse, P. Loiko, C. Grygiel, A. Benayad, F. Lemarie, V. Zakharov, A. Veniaminov, J. L. Doualan, A. Braud, and P. Camy, "Liquid phase epitaxy growth, structure and spectroscopy of highly-doped 20 at.% Yb^{3+}:LiYF4 thin films," J. Lumin. **236**, 118071 (2021).
64. R. Galina Nemova and R. Kashyap, "Temperature dynamics of laser cooling of solids with Yb^{3+} ions," Proc. SPIE **9000**, 56–68 (2014).
65. Y. Z. Liu, U. Demirbas, M. Kellert, J. Thesinga, H. Cankaya, Y. Hua, L. E. Zapata, M. Pergament, and F. X. Kärtner, "Eight-pass Yb:YLF cryogenic amplifier generating 305-mJ pulses," Osa Contin. **3**(10), 2722–2729 (2020).
66. U. Demirbas, H. Cankaya, Y. Hua, J. Thesinga, M. Pergament, and F. X. Kärtner, "20-mJ, sub-ps pulses at up to 70 W average power from a cryogenic Yb:YLF regenerative amplifier," Opt. Express **28**(2), 2466 (2020).
67. U. Demirbas, H. Cankaya, J. Thesinga, F. X. Kärtner, and M. Pergament, "Power and energy scaling of rod-type cryogenic Yb:YLF regenerative amplifiers," J. Opt. Soc. Am. B **37**(6), 1865–1877 (2020).
68. H. Cankaya, U. Demirbas, Y. Hua, M. Hemmer, L. E. Zapata, M. Pergament, and F. X. Kärtner, "190-mJ cryogenically-cooled Yb:YLF amplifier system at 1019.7 nm," OSA Continuum **2**(12), 3547–3553 (2019).
69. A. P. Savikin, N. A. Egorov, N. G. Zakharov, O. N. Eremeĭkin, and V. V. Sharkov, "Investigating a thermal lens in a Tm:YLF crystal under intense diode pumping," J. Opt. Technol. **76**(11), 676–679 (2009).
70. J. Liu, X. Chen, Y. Yu, C. Wu, F. Bai, and G. Jin, "Analytical solution of the thermal effects in a high-power slab Tm:YLF laser with dual-end pumping," Phys. Rev. A **93**(1), 013854 (2016).
71. B. Fang, H. Zhulong, L. Jingliang, C. Xinyu, W. Chunting, and J. Guangyong, "Thermal analysis of double-end-pumped Tm:YLF laser," Laser Phys. **25**(7), 075003 (2015).
72. N. P. Barnes and D. J. Gettemy, "Temperature variation of the refractive indices of yttrium lithium fluoride," J. Opt. Soc. Am. **70**(10), 1244–1247 (1980).

Optical Materials EXPRESS

73. O. S. Kazasidis and U. Wittrock, "Interferometric measurement of the temperature coefficient of the refractive index dn/dT and the coefficient of thermal expansion of Pr:YLF laser crystals," Opt. Express **22**(25), 30683–30696 (2014).
74. V. Pilla, P. R. Impinnisi, and T. Catunda, "Measurement of saturation intensities in ion doped solids by transient nonlinear refraction," Appl. Phys. Lett. **70**(7), 817–819 (1997).
75. B. W. Woods, S. A. Payne, J. E. Marion, R. S. Hughes, and L. E. Davis, "Thermomechanical and thermooptic properties of the $LiCaAlF_6$-Cr^{3+} laser material," J. Opt. Soc. Am. B **8**(5), 970–977 (1991).

217.93.245.72 ts 2022-06-09 15:36:57